# Equilibrium and Stability of High-Beta Plasmas in Wendelstein 7-AS

M.C. Zarnstorff[1], A. Weller[2], J. Geiger[2], A. Reiman[1], A. Dinklage[2], E. Fredrickson[1], G.-Y. Fu[1], S. Hudson[1], J. Knauer[2], L.P. Ku[1], D. Monticello[1], C. Nührenberg[2], A. Werner[2], the W7-AS Team and NBI-Group.

[1]*Princeton Plasma Physics Laboratory, Princeton, NJ 08543 USA*
[2]*Max-Planck Institute for Plasma Physics, EURATOM Assoc., D-17491 Greifswald, Germany*

e-mail contact of main author: zarnstorff@pppl.gov

**Abstract.** Quasi-stationary, MHD-quiescent discharges with volume averaged beta-values up to 3.4% were sustained in the W7-AS for more than 100 energy confinement times. A stability limit was not observed. The achieved beta appears to be limited by confinement, but is sensitive to the magnetic configuration. The decrease in beta for vacuum rotational transform < 0.5 is consistent with an equilibrium beta-limit given by a Shafranov axis-shift of one-half the minor radius. The plasma equilibria are reconstructed, fitting the magnetic diagnostic measurements and the Thomson-scattering pressure profile, using a modified version of the STELLOPT. Analysis of the free-boundary equilibria by PIES indicate that the beta-limit and its variation may be due to deterioration of the flux surfaces and generation of magnetic stochasticity. Low-frequency n =1 and 2 MHD activity is often observed at intermediate beta-values, but does not impede access to higher-beta. Linear ideal-MHD free-boundary stability calculations indicate that the mode should be unstable for beta < 2.5%, and thus severely underestimate the achievable beta-limit.

## 1. Introduction and plasma characteristics

Achieving high plasma pressure in stationary plasma conditions, without disruptive activity, is a key challenge for developing fusion energy. Quasi-stationary, quiescent discharges with volume averaged beta ⟨β⟩-values up to 3.4% were achieved in the W7-AS stellarator [1]. The processes that limit the accessible β values are investigated to develop an understanding of 3D stability and the expected operating limits for new experiments.

The highest β values in W7AS were obtained at low magnetic field B=0.9 – 1.05 T and a vacuum rotational transform $\iota_{ext} \sim 0.5$. A typical example is shown in Fig. 1, where a ⟨β⟩ = 3.4% plasma is maintained in steady conditions, heated by 3.9 MW of co-tangential hydrogen neutral beam injection into a hydrogen plasma. The total plasma current was feedback controlled to be approximately zero, using a small Ohmic current to cancel the net bootstrap and beam-driven current. The line-averaged electron density $\bar{n}_e \sim 2.4\times10^{20}$ m$^{-3}$, and the plasma has the characteristics of the HDH enhanced confinement regime [2]. These high-β plasmas were only obtained after the island divertor structures were installed. However, the divertor control coils are energized to suppress edge islands and maximize the plasma volume, so an island divertor

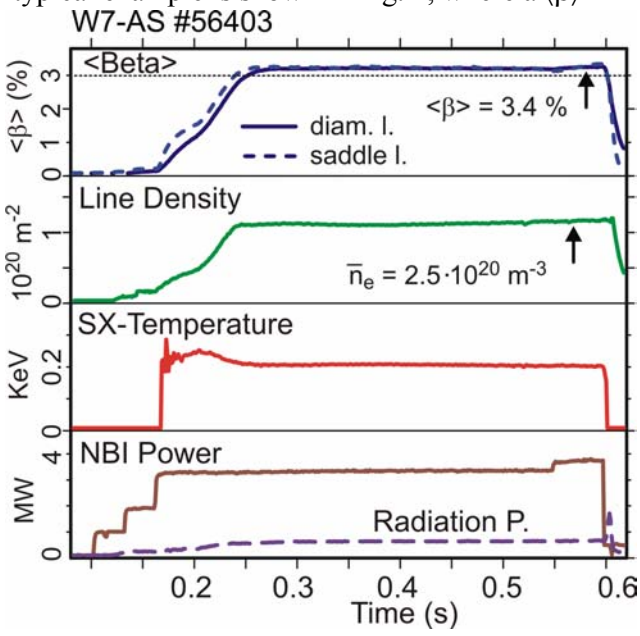

edge configuration was not expected.

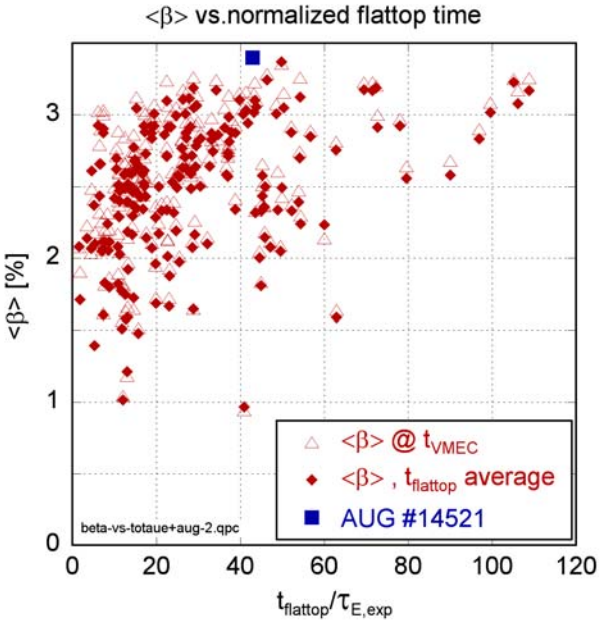


During the high-β phase, the plasma are typically quiescent and large-scale MHD activity is not apparent. The plasma pressure was maintained as long as the heating power was supplied or until the power handling capability of the plasma-facing components was exceeded, leading to an uncontrolled increase in radiated power and loss of stored energy. As shown in Figure 2, the maximum β was approximately independent of pulse length and was maintained for more than 100 energy confinement times. A stability limit was not observed, and the maximum beta was not limited by the onset of observable instabilities. The β values achieved appear to be limited by confinement and heating power, but are sensitive to the magnetic configuration. W7AS had a flexible coil set, with toroidal field coils for varying the rotational transform $\iota$, special modular coils for varying the toroidal mirror ratio, island-divertor control coils, and vertical field coils in addition to the main modular coils. All of these modify the magnetic configuration and affect the achieved β.

Figure 3 shows the observed variation of β with $\iota_{ext}$. For $\iota_{ext} < 0.5$, the achieved β is large enough that the expected Shafranov shift [3] of the magnetic axis approaches <a>/2, half the average minor radius, which is the classical equilibrium limit. The decrease of β for $\iota_{ext} > 0.5$ contradicts the standard expectation that increased $\iota$ should provide increased global energy confinement and increased stability. Similarly, Figure 4 shows the variation of β with the divertor control-coil current, $I_{CC}$. The control-coils were designed to make a resonant magnetic perturbation for control of edge islands, and are calculated to have no effect on $\iota$ or on the neoclassical ripple transport in the collisionless regime. Yet, they strongly affect the quiescent β value, in plasmas showing no strong MHD activity. Thus, there are strong indications that other characteristics of the plasma equilibrium control the accessible β.

## 2. Equilibrium reconstruction

An accurate reconstruction of the plasma equilibrium is required to understand these high-β plasmas and compare them to theoretical models. This includes a determination of the profiles of the plasma pressure and $\iota$ including the effect of plasma currents. The data readily available on W7AS include a 45-point Thomson scattering system, and 19 magnetic diagnostics (two diamagnetic loops at different toroidal positions, a Rogowski loop, a 4-segment Rogowski array, and 12 saddle loops of 3 shapes). The integration of the magnetic diagnostics starts after the magnetic fields reach their programmed values, and they are compensated for residual noise variations of the field coil currents. Thus, the diagnostics only measure the plasma-induced signal. The uncertainty of the magnetic measurements is estimated to be ±3%, due to uncertainties in location and shape. The electron pressure profile shape measured by Thomson scattering characterizes the total pressure profile shape, as that the ion and electron temperatures are strongly equilibrated due to the high plasma density,

$n_e(0) > 10^{20}$ cm-3. The non-thermal beam stored energy is estimated to be less than 5% of the total plasma energy.

The stellarator design-optimization code STELLOPT [4] has been modified to reconstruct the W7AS equilibrium self-consistently. STELLOPT uses the free-boundary inverse-equilibrium solver VMEC [5] to calculate the 3D plasma equilibrium given specified coil currents and plasma pressure and current profiles, which are represented as polynomials in the normalized toroidal flux. VMEC assumes that the equilibrium has nested toroidal flux-surfaces. An improved Levenberg-Marquardt search is used to adjust the profiles or other free parameters to minimize the RMS-deviation of specified criteria with specified weights. To serve as a reconstruction code, STELLOPT was modified to target the experimental conditions, thus providing a least-squares fit to the available diagnostics. The modifications include: (1) Adjusting the plasma size to minimize the separation between the plasma surface and a set of piecewise-linear limiting surfaces at specified toroidal angles, representing the many in-vessel structures present in the experiment. (2) Adjusting the pressure polynomial coefficients to match a set of measured pressure data points at arbitrary 3D laboratory coordinates, which are used to specify the Thomson scattering measurements.. Only the shape of the measured profile is used, the amplitude is adjusted to match the magnetic diagnostics, or the diamagnetic stored energy (if not fitting to magnetic measurements directly). (3) Adjusting the current and pressure polynomial coefficients to match the set of magnetic diagnostic measurements with simulations calculated by the DIAGNO code [6] using the VMEC equilibrium solution. The weights for the fit are set to be the inverse of the one-standard-deviation uncertainty in each of the measurements.

STELLOPT iterates the fit using fully-converged VMEC equilibrium solutions. Thus, this technique is computationally expensive compared to tokamak equilibrium reconstruction codes, or the approach being implemented in the V3FIT project [7,8]. A typical analysis requires 2-3 hours on a 16-CPU cluster. However, the computation inefficiency is balanced by the ease of incorporating additional diagnostics and the extensive set of theoretical models already available from the design-optimization studies.

The information content of the magnetic diagnostics has been investigated by principal component analysis of a database of simulated equilibria using methodically varied profiles, but no total toroidal current. An earlier analysis [9] of the W7AS magnetic diagnostics found six significant principal components, but did not attempt to distinguish between profile and magnetic configuration information. All the magnetic diagnostics respond strongly to the plasma energy. The diagnostic response at fixed plasma energy and for a fixed set of coil currents was analyzed, finding two significant empirical orthogonal functions (EOF) together accounting for 99.9% of the variance due to variations of the pressure profile shape. There is only one EOF that accounts for all the variance due to changes of the current profile shape. The detailed form of the EOFs appears to depend on the fixed plasma energy analyzed. This may be due to the non-linearity of the equilibrium equation.

Figure 5 shows the pressure and current profiles for the b=3.4% plasma of Figure 1, from the fit to the Thomson scattering and magnetic diagnostic measurements. The pressure profile was fit by a 10-term polynomial, using an $11^{th}$ term to constrain the edge pressure to zero. The Thomson scattering measurements show considerable scatter, leading to a high $\chi^2_{TS}$ of approximately 3 per Thomson data point. This is dominated by the single-point discrepancy at

R=2.11m. The total plasma energy from the fitted pressure profile agrees with the diamagnetic loop energy analysis, with a difference of less than 2%.

The current profile was fit using a 3-term polynomial, since the magnetic diagnostics are only sensitive to one current profile shape EOF and the total current. The resulting $\chi^2_{mag}$ for the magnetic diagnostic is 0.83 per diagnostic. The diagnostics cannot distinguish between profiles with finite edge current density, or ones constrainted to have no edge current-density, as shown in Fig. 5. Fits using 4 or 5 moments did not improve the fit or change the appearance of the current profile. Use of more than 5 moments led to solutions with large alternating-sign coefficients and large radial oscillations in the current and $\iota$ profiles, indicating over-fitting. Figure 5 also shows a comparison between the fitted current profile and kinetic calculations [10] of the net current profile from the beam, bootstrap, and compensating ohmic currents. The fitted current has a similar shape to the calculated current profile, but is significantly larger. Imposing the calculated current current profiles would increase $\chi^2_{mag}$ by a factor of 1.8 – 2.4, thus they appear to be inconsistent with the magnetic measurements. The sensitivity of the magnetic diagnostics to the magnitude of the current profile is mainly through sensor coils 3 and 4 of the segmented Rogowski array, and saddle-loop 1 (to a lesser extent). The sensitivity of these measurements to changes in the magnitude of the current profile is shown in Fig. 6, indicating that the difference between the calculated and fit current profiles is significant.

**3. Equilibrium topology**

The large Shafranov shift of the magnetic axis, nearing a/2, and the sensitivity of the achieved β to the magnetic configuration, suggests that the plasma confinement and β may be influenced by details of the equilibrium, including the formation of islands and stochastic regions. To assess this, the dependence of the plasma β on the control coil current has been studied using the PIES code [11], which does not assume closed flux-surfaces. Free-boundary three-dimensional equilibria have been numerically calculated for the plasmas of Fig. 4, an experiment scanning only the control-coil current. The calculations use the pressure profile from the equilibrium reconstruction. $\langle\beta\rangle \sim 2.7\%$ was achieved with the optimum control-coil current ($I_{CC}$ = -2.5 kA), but this fell to $\langle\beta\rangle \sim 1.8\%$ for $I_{CC} = 0$. The PIES calculated equilibria for these cases indicate that the outer ~ 35% of the flux surfaces are stochastic in both plasmas at their (different) $\langle\beta\rangle$ values, see Fig. 7. Radial transport in the stochastic region may be enhanced due to transport parallel to the magnetic field, limiting the ability to access higher β. PIES equilibria were calculated as a function of $\langle\beta\rangle$, keeping the pressure profile shape fixed. Figure 8 shows that the calculated fraction of good flux

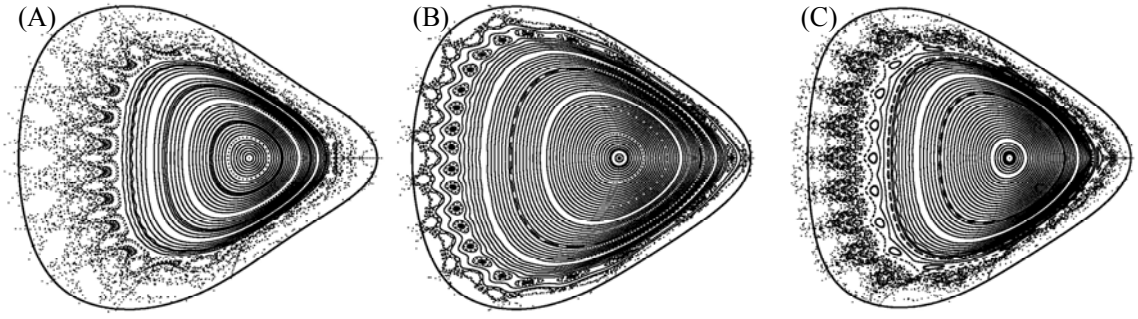


surfaces drops with increasing β for all cases, but the drop occurs at higher β for $I_{CC}$ = -2.5 kA than for $I_{CC} = 0$. In both cases, the fraction of good flux surfaces plunges slightly above the

achieved ⟨β⟩. Thus, the PIES equilibria indicate that the experimental β limit and its variation due to the control coil current may be due to deterioration of the flux surfaces and the effect of magnetic stochasticity on the plasma confinement.

The 3.4% plasma shown in Fig. 1 was obtained with $I_{CC}$=-2.95 kA but a lower magnetic field (0.9 T) than the plasmas in Fig. 4. Thus, the perturbation made by the control coil was ~40% stronger. The equilibrium for this case is presently being analyzed by PIES.

The PIES equilibrium calculations can also attempt to simulate the response of the plasma to changes in the flux surface topology by flattening the plasma pressure in any region calculated to have stochastic field lines or be inside an island. In this case, the non-linear evolution of the calculation progressively shrinks the plasma, so that the calculated equilibrium is fully stochastic and there is no pressure gradient for initial ⟨β⟩ ≥ 1% ($I_{CC}$ = 0) or ≥ 2% ($I_{CC}$ = -2.5kA). The disagreement between these collapsed equilibrium calculations and the observed plasmas with higher ⟨β⟩ indicates that a more sophisticated plasma response model is needed [12]

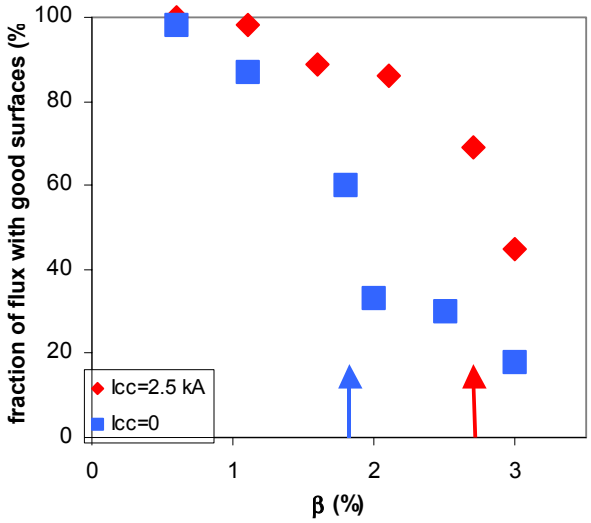


**4. MHD stability – low/medium n**

Low-frequency MHD activity with toroidal mode number n ≤ 2 is often, but not always, observed at intermediate β-values, 1.5% < β < 2.5%, during the increase in β after the increase of beam power. In most cases, these modes saturate without degrading plasma confinement or impeding access to higher-β values. Unfortunately, the pressure profile in this unstable phase was never measured with Thomson scattering. Linear ideal-MHD free-boundary stability calculations using CAS3D [13] for a plasma with $\iota_{ext}$ = 0.52, assuming a parabolic pressure profile, indicate that the m/n = 2/1 mode should be unstable for ⟨β⟩ < 2.5% [14, 3]. For higher β values, the resonant surface is no longer in the plasma. The observed MHD activity is approximately consistent with these stability calculations. These calculations have been confirmed using the Terpsichore [15] linear-stability code, for the reconstructed pressure profile of the plasma in Fig. 1. The m/n=2/1 mode is calculated to be unstable for 1% < β < 2.5%. At the flat-top ⟨β⟩ =3.4%, the plasma is calculated to be weakly unstable to a m/n=5/2 instability at the plasma edge. A saturated fluctuation is observed at 5 kHz on the Mirnov coils, but the mode-numbers cannot be unambiguously identified.

The linear-stability threshold for this plasma would typically be calculated to be ⟨β⟩ =1 – 1.5%, and the m/n=2/1 instability is often observed at approximately this β value. However, since this instability saturates and does not limit access to higher ⟨β⟩ values, the low-n linear stability threshold significantly underestimates the achievable β-limit.

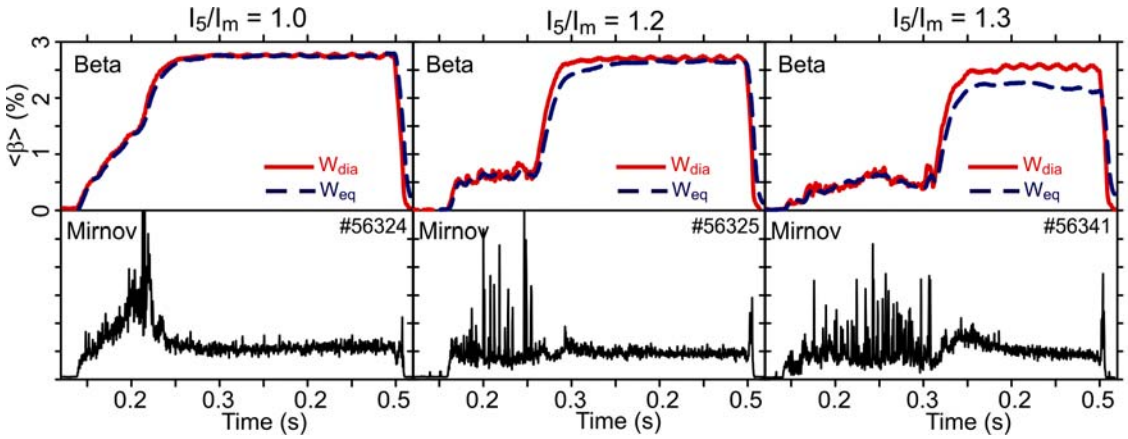


**5. MHD stability – high n**

The high beta plasmas discussed so far are calculated to be stable to high-n instabilities, provided the termperature is kept high enough to avoid resistive instabilities using the COBRA code [16]. For the bulk of the plasma profile, there is are no nearby stability thresholds, thus ballooning modes are not expected to limit the plasma β**.**

In Wendelstein 7-AS, the the toroidal magnetic field ripple or mirror depth can be varied by changing the current in the 'corner' modular coil ('$I_5$'). This also increases the vacuum magnetic hill, though finite plasma pressure generates a net magnetic well. Experiments in these configurations showed a bifurcated behavior. At the onset of neutral beam heating, frequent fast MHD bursts were observed and the plasma β was limited to ~ 0.6% for a prolonged period. Suddenly, the MHD bursts ceased and the β increased to ~2.7% similar to the standard configuration, as shown in Figure 9. The duration of the bursting period increased with increasing magnetic mirror ratio. Linear stability calculations of the ideal localized ballooning mode using COBRA indicated that the high β-phase appeared to be in the second-stability regime. This prompted an investigation of the evolution of the ballooning threshold during the increase in plasma pressure, to understand how the second-stable regime was accessed. Figure 10 shows stability diagrams [17] for a sequence of free-boundary equilibria with increasing β from left to right for the r/a=0.7 (half flux) surface. The dotted line shows the stability boundary for the symmetric field line passing through θ=0, φ=0, and the solid line shows the stability boundary envelope for the whole flux surface. The measured pressure profile is calculated to be in the second stable region inside of r/a ~ 0.8. From the calculated sequence of boundaries versus β, it appears that the plasma accesses the this region along a stable trajectory, due to an increase of shear with plasma pressure and a deformation of the stability boundary.

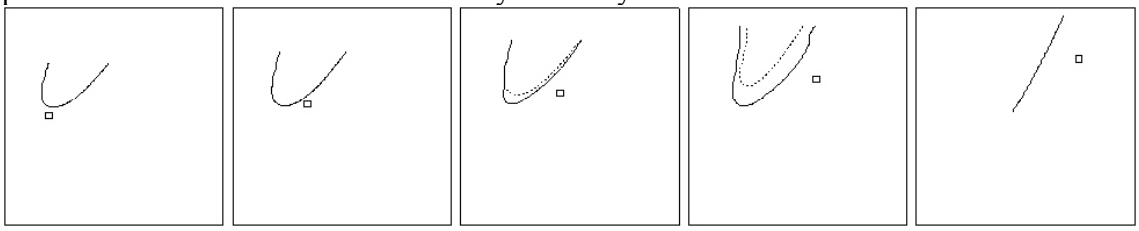

## 5. Summary

Quiescent quasi-steady plasmas with ⟨β⟩ up to 3.4% were achieved in W7-AS, and maintained for more than 100 energy confinement times. There was no indication of a stability limit, rather the achieved β appeared to be limited by energy confinement and heating power. The plasma equilibrium was reconstructed fitting external magnetic measurements and Thomson scattering measurement of the electron pressure profile. PIES calculations of the equilibrium indicates that a stochastic-field region forms at the edge of the plasma as b increases, and that the observed ⟨β⟩ value corresponds to a loss of approximately 30% of the flux. An abrupt loss of flux-surface integrity is predicted for β values above those observed. Thus, the onset of stochastic magnetic fields and the loss of good flux surfaces may control the transport and achievable ⟨β⟩ value.

These plasmas often experience m/n=2/1 instabilities at intermediate ⟨β⟩ < 2.5%, in reasonable agreement with linear instability calculations indicating a threshold of ⟨β⟩~1%. However, the instability saturates and does not inhibit access to high b values. Thus, the linear stability threshold is not a good indication of the β-limit.

**Acknowledgement**

We are grateful for the support and encouragement of Prof. T. Klinger, Prof. R. Goldston, and Dr. R. Nazikian. We would like to thank Dr. S.P. Hirshman, Dr. W.A. Houlberg, and Dr. A. Cooper for providing the VMEC, AJAX, and TERPSICHORE codes, respectively. This work was supported by U.S. DoE Contract DE-AC02-76-CHO-3073.

**Figure Captions:**

Figure 1.Time evolution of a quasi-stationary, quiescent plasma with ⟨β⟩ = 3.4%, B = 0.9T, $P_{NB}$=3.9 MW, $\iota_{ext}(0)$ = 0.47, and $I_{CC}$ = 2.96 kA. The Thomson scattering measurement time is indicated by the vertical dashed line.

Figure 2. Database plot showing ⟨β⟩ versus the sustained time-duration divided by the energy confinement time. The open symbols give the peak-⟨β⟩ value, and the closed symbols are the time-average value. The small difference between the symbols is an indication of the steady plasma conditions.

Figure 3. Variation versus the external central rotational transform $\iota_{ext}(0)$ of (A) peak-⟨β⟩ and (B) amplitude of $\dot{B}$ fluctuations measured by an external Mirnov coil characterizing MHD activity, for B=1.25 T, $P_{NB}$ = 3.4 MW, and $I_{CC}$ = 2.5 kA.

Figure 4. Variation versus the divertor control-coil current $I_{CC}$, of (A) peak-⟨β⟩ and (B) amplitude of $\dot{B}$ fluctuations measured by an external Mirnov coil, for B=1.25 T, $P_{NB}$ = 3.4 MW and $\iota_{ext}(0)$ = 0.44.

Figure 5. For the plasma of Figure 1: (A) Measured pressure profile (points with one-sigma error bars) from Thomson scattering and fit profile from reconstruction, (B) Fitted current

profiles (solid) compared with kinetic calculations (dashed). (C) Rotational transform profile from equilibrium reconstruction (solid) and assuming no net toroidal current density (dashed).

Figure 6. Simulated signals for segmented Rogowski-array sensor coils 3 (A) and 4 (B) versus the relative magnitude of the current profile, where 1 represents the fitted current in Fig. 5. Also shown are the measured values and the range of uncertainty.

Figure 7. PIES calculated flux surface topologies at the triangular symmetry plane for two of the plasmas in Fig. 4: (A) $I_{CC}$=0 and $\langle\beta\rangle$ = 1.8%, (B) $I_{CC}$=-2.5kA and $\langle\beta\rangle$ = 2.0%, (C) $I_{CC}$=-2.5kA and $\langle\beta\rangle$ = 2.7%. In each case, the dark line is the STELLOPT/VMEC calculated plasma boundary.

Figure 8. Fraction of good flux surfaces versus $\langle\beta\rangle$ for two plasmas of Fig. 4: $I_{CC}$=0 and $I_{CC}$=-2.5kA

Figure 9. Time evolution of $\langle\beta\rangle$ and Mirnov signal for a plasma with $I_5/I_M$ = 1.3, showing initial unstable period followed by a transition to high-$\beta$.

Figure 10. Stability diagrams for the configuration of the plasma showing in Fig. 9, for r/a = 0.7 and various $\langle\beta\rangle$-values. In each diagram, $\iota$' is plotted versus p', the symbol indicate the measured value and the curve indicates the stability boundary for the flux-surface. The dashed curve indicates the stability boundary for the $\theta$=0, $\varphi$=0 field-line.

**References**

[1] A. Weller et al, IAEA Nuclear Fusion and Plasma Phys. 2002 (Lyon), paper EX/S3-1.
[2] K. McCormick et al., Phys. Rev. Lett. **89** (2002) 015001.
[3] J. Geiger et al., Fusion Sci. and Technology **46** (2004) 13.
[4] D. Strickler et al, IAEA Nuclear Fusion and Plasma Phys. 2002 (Lyon), paper FT/P2-06.
[5] S.P. Hirshman et al., Comput. Phys. Commun. **43** (1986) 143.
[6] H.J. Gardner, Nucl. Fusion **8** (1990) 1417.
[7] S.P. Hirshman et al., Phys. Plasmas **11** (2004) 595.
[8] N. Pomphrey et al, this conference, paper IC/P6-45.
[9] H.P. Callaghan, et al., 25th EPS Conf. on Contr. Fusion and Plasma Phys., Praha, ECA Vol. **22C** (1998) 1470.
[10] J. Geiger et al, 30th EPS Conf. on Contr. Fusion and Plasma Phys., St. Petersburg, ECA Vol. **27A** (2003) 1470.
[11] A.H. Reiman and H. Greenside, Compt. Phys. Commun. **43** (1986) 157.
[12] A.H. Reiman et al, this conference, paper IC/P6-46.
[13] C. Nührenberg, Phys. Plasmas **6** (1999) 137.
[14] A. Weller et al., Plasma Phys. Control. Fusion **45** (2003) A285.
[15] D.V. Anderson et al, Scient. Comp. Supercomputer **II** (1990) 159.
[16] R. Sanchez et al., J. Comput. Phys. **161** (2000) 589.
[17] S.R.Hudson and C.C.Hegna. Physics of Plasmas **10** (2003):4716.